Semnan University

Progress in Physics of Applied Materials

journal homepage: https://ppam.semnan.ac.ir/

# The effect of liquid nitrogen-microwave treatments on the structural, optical, and tribological properties of $WS_2$ nanoflakes

**M. Mahdavi[a], S. Kimiagar[b*], F. Abrinaei[c]**

[a]*Department of Physics, Central Tehran Branch, Islamic Azad University, Tehran, Iran.*
[b]*Nano Research Lab (NRL), Department of Physics, Central Tehran Branch, Islamic Azad University, Tehran, Iran.*
[c]*Department of Physics, East Tehran Branch, Islamic Azad University, Tehran, Iran.*

**ARTICLE INFO**

Article history:
Received: 13 September 2021
Revised: 13 November 2021
Accepted: 11 December 2021

Keywords:
Environmental friendly method
Freezing
Friction coefficient
Heating
Tribology
$WS_2$ nanoflakes

**ABSTRACT**

$WS_2$ was successfully synthesized by the hydrothermal method under various liquid nitrogen and microwave treatments. X-ray diffraction (XRD) analysis showed the presence of multiple $WS_2$ phases, of which hexagonal was the dominant phase. The morphology of the samples was examined by scanning electron microscopy (SEM) and transmission electron microscopy (TEM) and $WS_2$ exfoliation was confirmed after liquid nitrogen and microwave treatments. Fourier transform infrared spectroscopy (FTIR) confirmed $WS_2$ exfoliation during the exfoliation process. Optical bandgap calculation showed an increase in the exfoliation $WS_2$ bandwidth to 4.7 eV, which is large enough for the massive indirect bandwidth (1.3 eV) of $WS_2$, indicating the effect of quantum confinement. Decreased photoluminescence (PL) showed the production of defects in the samples during the processes. The tribological properties of $WS_2$ nanoflakes as an additive in oil showed that the coefficient of friction and wear performance of the oil were significantly improved by adding $WS_2$ nanoflakes synthesized by the hydrothermal method under different liquid nitrogen and microwave treatments. The results show that $WS_2$ nanoflakes with an improved coefficient of friction and wear performance can be a promising additive that could open a new avenue for the large-scale production of tribological materials.

## 1. Introduction

Lubricating materials play a significant role in the myriad of devices that are essential in everyday life due to the reduction of high friction and the minimization of abrasion between surfaces. Lubricants improve the energy efficiency of devices and increase the mechanical endurance of machines. Lubricating materials are used to reduce friction by forming a second layer between two surfaces that are in motion, thereby improving performance and efficiency.

Recently, scientists have turned their attention to improving the performance of lubricants to extend their service life by using a combination of lubricants that reduce friction and noise, prevent excessive wear, and protect against corrosion. Type of movement (sliding or rolling), speed (fast, medium or slow), and temperature in tribological systems along with load and operating environment Applications are important factors in selecting materials to optimize lubricant performance. Easy and cost-effective production, ease of use in the target equipment, and lifespan of lubricants are important to choosing materials for tribological applications.

Due to the ability to control the size and shape of nano-lubricants during the synthesis process, the use of nano-lubricants is very effective in the industry. In addition, nano-lubricants are very important in boundary lubrication due to their lower coefficient of friction and high efficiency at room temperature [1, 2].

Recently, several studies have focused on developing tribological performance of nano-lubricants such as carbon-based nanostructures [3-6], $MoS_2$ [7-9], $WS_2$ [10-13], $TiO_2$ [14], and ZnO [15-17]. Taran et al. exfoliated and functionalized $MoS_2$ powder through freezing and thermal shock [18]. Wang et al. focused on organic-inorganic additives [19]. Lince et al. investigated solid lubricants [20]. Freschi et al. studied Micro-and Nano-$WS_2$ Structures [21]. Fayaz et al. examined the tribological behavior of $WS_2$ nanoparticles [22]. Wu et al. investigated anti-wear features of $WS_2$ particles and ZDDP [23]. Zhu et al. used the liquid-nitrogen and microwave method to exfoliate bulk layered materials into the ultrathin 2D structure [24].

* Corresponding author. Tel.: +989121230921
*E-mail address:* s_kimiagar@iauctb.ac.ir

DOI: 10.22075/PPAM.2021.24535.1015

However, transition-metal dichalcogenides (TMDs) nanomaterials such as $MoS_2$ and $WS_2$ have been favored by some researchers because of their layered structure [7-13]. TMDs nanomaterials have the $MX_2$ standard structural formula, where M denotes a transition metal from groups IV-VI and X demonstrates a chalcogen atom alike S, Se, or Te [25]. Strong covalent forces exist between the interlayer M-X bonds, whereas adjacent layers are coupled through weak van der Waals forces that make cleaving along with the layers easy.

Among the various techniques developed for the preparation of $WS_2$ nanostructures, the hydrothermal process offers several advantages including environmental compatibility, one-step, and cost-effective synthesis process, relatively smooth operating conditions, good dispersion in solution, and the ability to produce crystalline phases. which is safely stable at higher temperatures. [26, 27].

Studies show that liquid phase peeling is a more efficient layer material, but the obtained exfoliated nanosheets are very low [28]. Water or other low boiling point solvents such as acetone and ethanol are probably good candidates for TMDs exfoliate. In such methods, the physical and chemical properties of $WS_2$ sheets are potentially affected because of impurities or defects due to the presence of surfactant in both peeling and purification stages [29]. Some studies have suggested the possibility of exfoliating TMDs in ethanol/water mixtures efficiently. [30, 31]. In addition, some researchers have proposed a method for exfoliating two-dimensional layered systems using solvent interpolation and microwave irradiation [32, 33]. In this study, we chose $WS_2$ because it has a layered structure. $WS_2$ was synthesized using the hydrothermal method. Then we introduced a more efficient method for peeling, which was freezing with liquid nitrogen and heating with a microwave. As far as we know, this is the first time this method has been used for $WS_2$ exfoliation. WS2 exfoliation via thermal shock is of interest for the large-scale synthesis of monolayer crystals. To confirm the peeling, the morphology of $WS_2$ nanoflakes was studied. The optical bandgap distance of $WS_2$ nanoflakes changed due to exfoliation. The potential of $WS_2$ nanoflakes as lubricant additives was investigated with the aim of industrial production of more efficient lubricants. This method leads to the loss of $WS_2$ properties due to structural changes during the exfoliation process.

## 2. Experimental details

All materials in these experiments were purchased from Merck Company. $WS_2$ nanoflakes were synthesized using the hydrothermal method. For solution one, 10 g Thiourea ($CH_4N_2S$) was dissolved in 200 mL ethanol while being stirred for 15 min at 80° C. In solution two, 6 g Sodium tungstate ($Na_2O_4W,2H_2O$) was separately dissolved in 200 mL ethanol while stirring was applied for 15 min at 80° C. Afterwards, some drops of Boric acid ($H_3BO_3$) were added to the second solution. Boric acid plays a key role as a reducing reagent during the reaction process. Solutions one and two were poured into a container at 80 ° C for 30 minutes and then transferred to a stainless steel autoclave reactor with a 420 mL Teflon coating. The reaction was performed at 180°C for 18 h. After cooling down to room temperature, the achieved powder was washed with ethanol (twice) and dried in a vacuum oven at 60 °C. The $WS_2$ powder was achieved. To exfoliate $WS_2$, 4 g of the obtained powder was dispersed in 20 mL ethanol and put in an ultrasonic bath for 30 min. The resultant solution was exposed to thermal shock by cooling in liquid nitrogen and then heating with microwave irradiation under 900 W powers. Liquid nitrogen was poured onto the solution to -120°C. The container containing the solution was immediately placed in the microwave for one minute. After one minute, the solution was removed from the microwave at a temperature of 70°C. The liquid-microwave nitrogen process for the solution was repeated. It means liquid nitrogen-microwave (first time) liquid nitrogen-microwave (second time) were applied. Then, the solution was dried in a vacuum oven at 40 °C. The achieved powder was labeled $WS_2$-2. In the next step, another sample was prepared with four rounds (four times) of liquid nitrogen-microwave. The resultant powder was tagged $WS_2$-4. To investigate the anti-wear property of the $WS_2$ nanoflakes as an additive for lubricating oils, we prepared three containers including 500 mL of the oil (T-68, DIN-51524 part II HLP). This oil is from Behran Company, which is used for industrial equipment. Then 0.02 g/L off the samples $WS_2$, $WS_2$-2, and $WS_2$-4 were dispersed in the container separately. Then, it was placed in the ultrasonic bath for 4 h to achieve a homogeneous solution. The Oil (0) and Oil (1) referred to the pure oil without any nanomaterial and the $WS_2$ nanoflakes additive, respectively. Similarly, the Oil (2) and Oil (4) were attributed to the $WS_2$-2, and $WS_2$-4 nanoflakes additives, respectively. The $WS_2$ performance in aqueous phase reactions is limited by its hydrophobicity while it improved for $WS_2$-2 and $WS_2$-4. This method for the exfoliation of $WS_2$ enhanced the dispersibility of the $WS_2$-2 and $WS_2$-4 samples.

## 3. Characterization

X-ray diffraction (XRD) was utilized to study the structure of the samples using X'Pert PRO, Philips with Cu–Kα radiation (λ = 0.154 nm). The Fourier transform infrared (FTIR) spectroscopy was applied using a spectrophotometer (FTIR) (Jasco -410) from 500 to 4000 $cm^{-1}$. The morphology of the samples was investigated by scanning electron microscopy (SEM) (XL30) and transmission electron microscopy (TEM) (Philips XL). The bandgap of the samples was calculated from Ultraviolet-visible (UV-Vis) optical absorption and transmission spectra (Lambda 750). Photoluminescence (PL) spectrum was recorded by a fluorescence spectrometer (PerkinElmer LS 45). The stability of the samples was measured by Zeta potential analyzer (Sabino, Particle Matrix). A homemade four-ball tribometer was used to evaluate the coefficient of friction and wear scars of the prepared samples. Alborztadbirkaran Iranian Company monitored the oil analysis situation. The temperature dependence of kinematic viscosity at 40 and 100˚C was determined using the ASTM D2270 method.

## 4. Results and discussion

XRD analysis was performed to determine the crystalline phases of $WS_2$ structures. Fig. 1 shows the XRD patterns of $WS_2$, $WS_2$-2, and $WS_2$-4 nanoflakes. The multiplicity of diffraction peaks in Fig. 1 implies the presence of multiple planes in the structures. The $WS_2$ crystals mainly consist of three crystalline phases: hexagonal-2H (anti-parallel), rhombohedral-3R (parallel), and octahedral (1T); the first two phases are semiconductors while the third phase is expected to be metallic. The rhombohedral-3R phase is more stable than the hexagonal phase -2H, while the octahedral phase (1T) is unstable as a bulk form and is associated only with the TMD monolayer[34]. Electron irradiation or introducing Lithium ions causes the phase transition from hexagonal to octahedral 1T [35].

Most peaks in the diffraction patterns correspond to the crystalline hexagonal structure based on JCPDS 00-002-0131 and 08-0237, P63/ MMC space group, 2H-$WS_2$. It means the hexagonal phase is dominant. The diffraction peak of (002) plane of hexagonal $WS_2$ is located at 2θ=15 and the other peaks at 29, 32, 33, 39, 50, 59, and 60, corresponding to (004), (100), (101), (103), (105), (008), and (112) planes of the hexagonal $WS_2$, respectively [36-38]. The (018) belongs to rhombohedral (JCPDS 084-1399, R3 m space group).

The reflection assigned to the (101) plane of $WS_2$-2 has higher intensity, though the diffraction peak matching with the (002) plane is broader, which could be ascribed to less exfoliation of $WS_2$-2 layers [36]. The sharp peaks matching with the (002) and (101) planes indicate competitive development of the crystallites along with these directions. The crystal lattice parameters of hexagonal structure can be found as a = b = 3.17 A° and c = 12.29 A°. The shift towards bigger angles can be seen for $WS_2$-2 and $WS_2$-4 samples. This indicates that the number of stacks in the layer of the $WS_2$ nanoflakes was reduced and the interspace of layers became larger [39].

However, the 1T-$WS_2$ does not show a well-defined structure. Applying XRD for characterizing the 1T-$WS_2$ is not easy. The peaks with circle sign in Fig. 1 can be attributed to the octahedral 1T phase of $WS_2$ [40, 41]. Sharma et al. [42] reported similar results. These diffraction peaks are more intense in the $WS_2$-2 sample suggesting that this sample is more metallic. The XRD results show that the preparation process has a direct effect on the phase transition of $WS_2$. There are some small peaks, which do not belong to any of the phases. This may be related to substances without reaction..

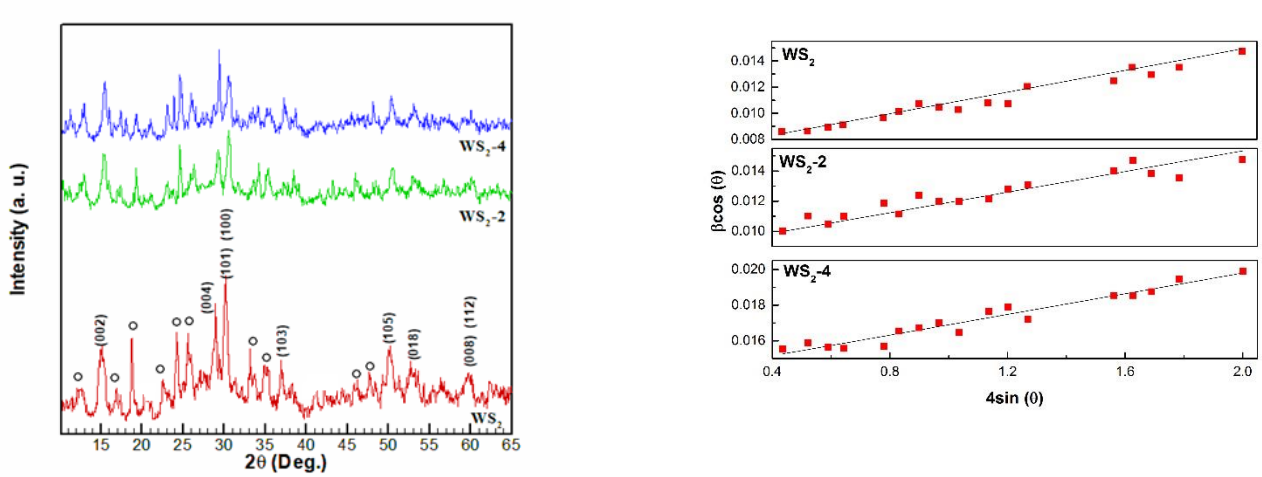


**Fig. 1**. XRD patterns of $WS_2$, $WS_2$-2, and $WS_2$-4 nanoflakes (left), Williamson & Hall calculation result (right)

To calculate the microstructural parameters for samples with high XRD peaks, the Williamson and Hall method is a suitable method that has been used to calculate the average crystal size of $WS_2$ nanoflakes. The Williamson & Hall equation is given below:

$$\beta\ cos\theta = 0.9\lambda/D + 4\varepsilon\ sin\theta \quad (1)$$

Where β is the estimated correct broadening of the sample in radian, θ is the diffraction angle, λ is the incident X-ray wavelength equal to 0.15406 nm, D is the average crystallite size in nanometers, and ε is the average strain. According to Williamson and Hall's method, when βcosθ is plotted against 4sinθ, the average values of crystal size can be estimated by fitting a line that intercept is equal to 0.9λ/D. The crystallite size values for the $WS_2$, $WS_2$-2, and $WS_2$-4 samples were estimated to be 20.86, 16.24, and 9.84 nm, respectively (Fig. 1 right).

Figure 2 illustrates the FTIR spectra of the synthesized $WS_2$ samples. The bands positioned at 600 and 900 $cm^{-1}$ are attributed to the W-S bond and S–S bond, in the respective order [43]. The band found at 1400 $cm^{-1}$ is attributed to the stretching vibrations of the hydroxyl group [43]. The bands at 1620 and 3200 $cm^{-1}$ are related to the W–S bending vibration and stretching vibration [44]. In addition, the vibrating bands at 2100 $cm^{-1}$ can be attributed to the atmospheric OH found in the $WS_2$ specimen [43]. The hydroxyl bending vibration and H–O–H stretching vibration matching with hydrogen bonding water is observed at 3450 $cm^{-1}$. The H–O–H and O–H peaks originate from interlayer water. Water molecules try to be between the layers of $WS_2$ material, which are joined together by

weak Vander Waal's forces [45, 46]. This demonstrates the successful exfoliation of $WS_2$ nanoflakes.

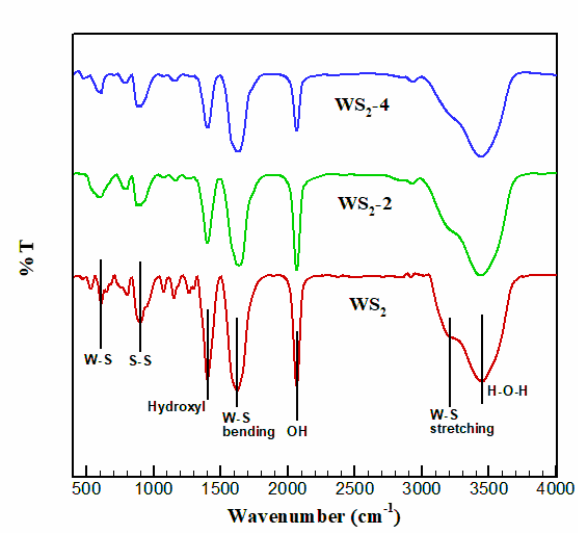


**Fig. 2.** FTIR spectra of $WS_2$, $WS_2$-2, and $WS_2$-4 nanoflakes

The quality characteristics of the synthesized $WS_2$ nanoflakes were evaluated through morphological and structural properties. $WS_2$ thin nanoflakes are shown in Fig.3. The sample population seems to include 2D-extended nanostructures with smooth surfaces and uniform thickness. The reduction of layers is evident in Fig. 3b. Fig. 3c shows that $WS_2$ nanoflakes are composed of a large number of small $WS_2$ nanoflakes.

TEM was used to further characterize the material. The products are clusters of nanoflakes with star shapes (Fig 4a). Fig 4b shows that $WS_2$ thin nanoflakes begin to peel, as seen in materials with layered structures. There are also grades of $WS_2$ exfoliating nanoflakes (Fig 4c). $WS_2$ thin nanoflakes are observed, indicating exfoliation of $WS_2$ after application of the liquid-nitrogen and microwave method.

The absorption spectra of $WS_2$ samples are shown in Fig. 5a. The general characteristics of the massive $WS_2$ adsorption spectrum are consistent with other reports [47, 48]. As seen in Fig. 5b, the WS2 spectrum shows the four characteristic peaks at 650, 580, 460, and 390 nm (labeled as A, B, C, and D), respectively. The peaks at around 650 and 580 nm are attributed to the excitonic absorption arising from direct bandgap transitions at the K point, meanwhile, the peaks located at around 390 and 460 nm are assigned to the optical transitions from the valence band to the conduction band. A shift to the higher wavelength is observed for two exciton bands when compared to the corresponding bands at 635.8 and 525.3 nm, reported for the bulk 2H $WS_2$ system [49]. The redshift in the peak position may occur due to the overlap with high-energy excitonic absorptions (A & B), excited states of excitons (C & D), and strong electron-phonon coupling, which gives rise to continuous absorption [50]. By reducing the size, the excitonic peaks fade, and the band edge shifts to a shorter wavelength [51]. The peak at around 230 nm is detected because of the small size surface defects of the $WS_2$ [52, 53]. It is believed that the bandgap differs by quantum confinement effects based on the size [53, 54]. It means that the smaller size leads to the bigger bandgap energy. Therefore, the strong quantum confinement effect leads to an enhancement in the bandgap. Interestingly, $WS_2$ bandgap is transformed into direct bandgap from indirect bandgap, with thickness reducing to monolayer or few layers from bulk [55]. The Tauc equation is $\alpha h\nu = A(h\nu - E_g)^n$, where $\alpha$ is the absorption coefficient of the material. The absorption coefficient of $WS_2$ nanoflakes can be calculated from UV-Vis data by using the Beer-Lambert formula, $\alpha = 2.303A/l$, in which A is the absorbance and l is the cell thickness. The value of n=1/2 is for direct allowed transitions and n=2 is for indirectly allowed transitions.

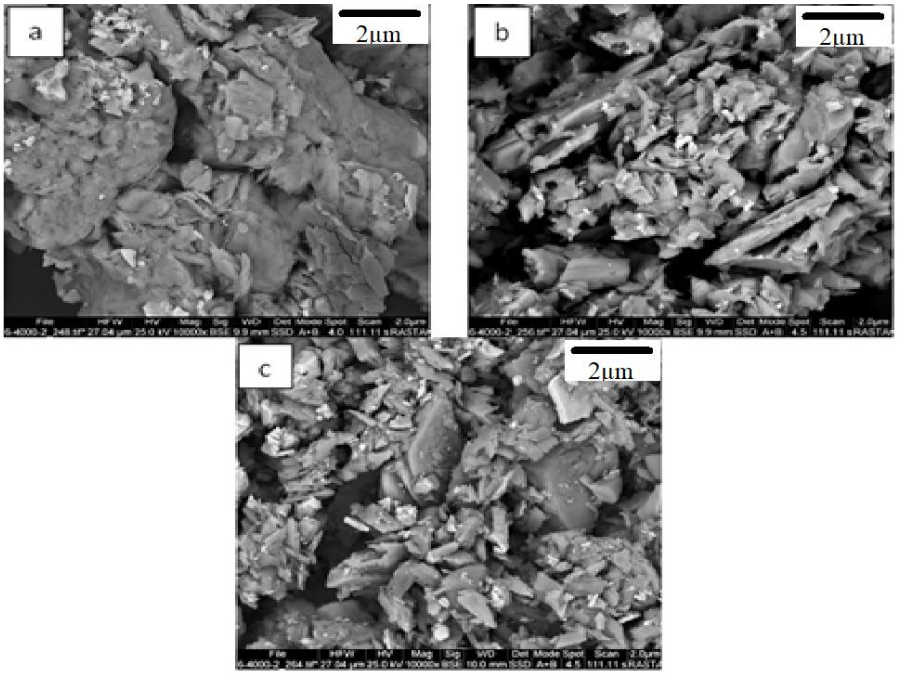


**Fig. 3.** SEM images of a) $WS_2$, b) $WS_2$-2, and c)$WS_2$-4 nanoflakes

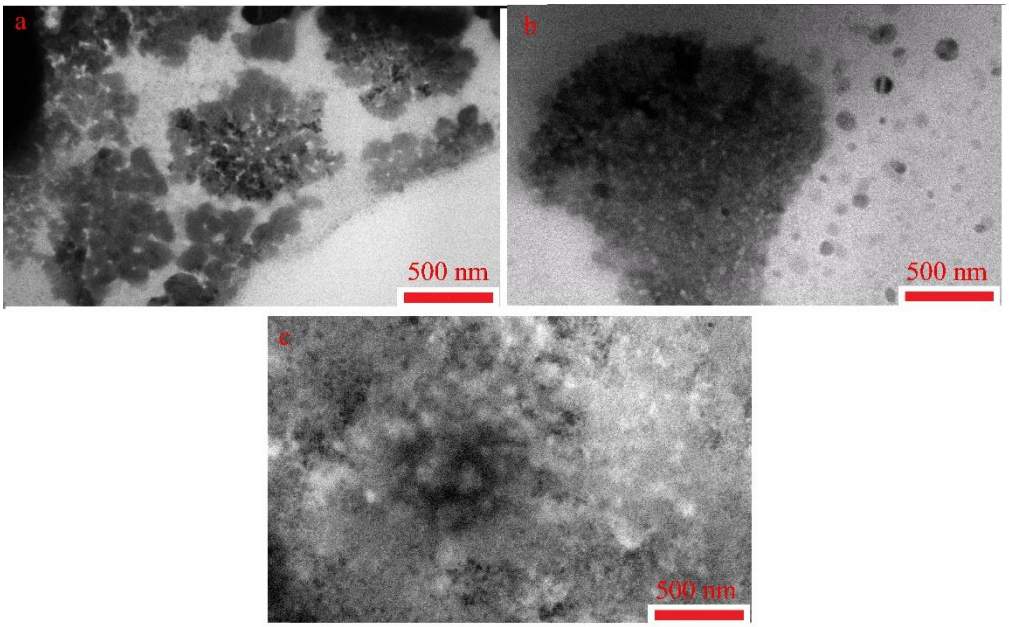


**Fig. 4.** TEM images of a) $WS_2$, b) $WS_2$-2, and c)$WS_2$-4 nanoflakes

By plotting the Tauc plot, the direct bandgap energy is determined at 4.65, 4.55, and 4.70 eV for $WS_2$, $WS_2$-2, and $WS_2$-4, respectively (Fig. 5c). It is much larger than the reported bandgap for bulk $WS_2$ (1.2 eV) [56] and monolayer $WS_2$ (2.1eV) [57]. Such a large enhancement in bandgap in semiconducting nanostructures is predicted and it is attributed to quantum confinement [58].

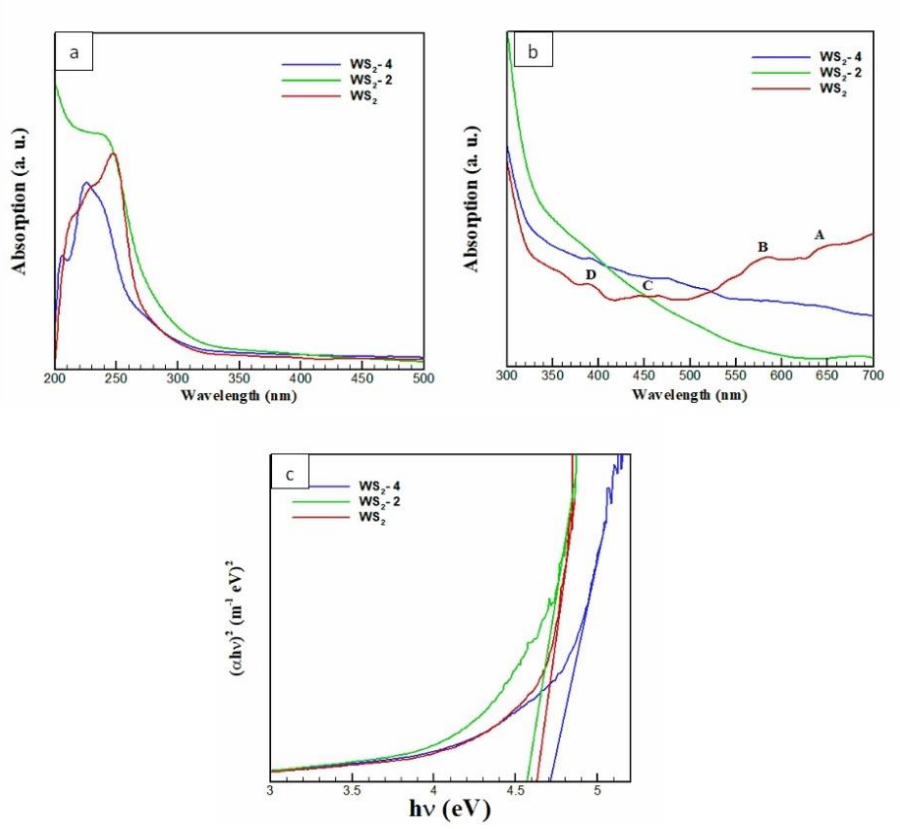


**Fig. 5.** a) UV-Vis spectra b) enlarged UV curve between 300 nm up to 700 nm, and c) the optical bandgap energy of the samples

Figure 6 displays the PL spectra of the $WS_2$, $WS_2$-2, and $WS_2$-4 at an excitation wavelength of 300 nm. A strong PL emission peak at around 450 nm is observed, which is consistent with other reports [59]. This peak is probably caused by the recombination due to excitons bound to different defects and/or surface states [60-63]. The PL reduction could be described by the generation of defects during the processes, which produced non-radiative centers and weakened the PL intensity. Another likely description of the PL reduction is the non-radiative recombination via the Auger effect as the Auger processes are very efficient in TMDs [64]. Moreover, the variation of the temperature and strain causes quenching and redshift in PL [65].

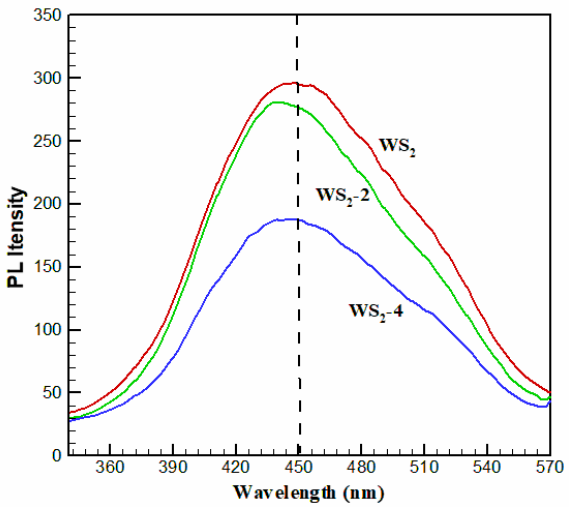


**Fig. 6.** PL spectra of $WS_2$, $WS_2$-2, and $WS_2$-4 nanoflakes

To study the long-term stability of additives in oil dispersion, eta potential was utilized after one day and two weeks (Fig. 7). Particles with low zeta potential values have high degrees of stability due to van der Waals interactions between particles and particles with zeta potential values greater than 30 mV. Zeta potential information is shown in Table 1. Obviously, after two weeks, there is a slight change in the zeta potential, which means no accumulation. Measurement of zeta potential shows better dispersion stability at 27 °C (58 mV) for $WS_2$-4 which has high stability.

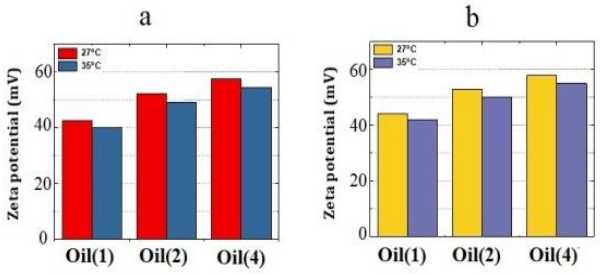


**Fig. 7.** Zeta potential of the oils after a) two weeks and b) one day

The main cause of energy loss in a mechanical system is friction, which can be decreased by lubrication. Therefore, it is important to choose the right combination of base oils and additives to improve the lubrication properties. By decreasing the coefficient of friction through friction modifiers, less fuel is consumed. Most of these modifiers have a layered format that allows the particles to slide smoothly on top of each other.

**Table 1**
The extracted data from Fig. 7

| Sample | Zeta potential after one day (mV) | | Zeta potential after two weeks (mV) | |
|---|---|---|---|---|
| | 27 °C | 35 °C | 27 °C | 35 °C |
| Oil(1) | 44 | 42 | 42 | 40 |
| Oil(2) | 53 | 50 | 52 | 49 |
| Oil(4) | 58 | 55 | 57 | 54 |

Figure 8 shows a schematic of a four-ball tribometer used to study the friction coefficient and wear scar of the as-prepared samples [66].

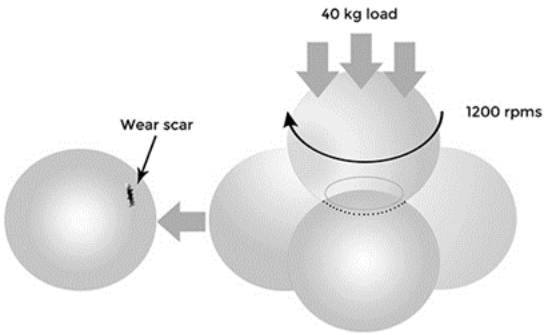


**Fig. 8.** Schematic of a four-ball test machine

Figure 9 shows the friction coefficient as a function of time for all lubricants containing $WS_2$, $WS_2$-2, and $WS_2$-4. As can be seen in Fig. 9, the addition of $WS_2$ reduces the friction coefficient compared to the base oil without an additive. Continuation of this reduction trend is also observed for $WS_2$-2, and $WS_2$-4 additives. As a result, the presence of $WS_2$-4 can lead to a significant reduction in friction coefficient and show a better lubricating performance. As predicted, these results show that the $WS_2$-4 is suitable and could help the lubricant via friction reduction.

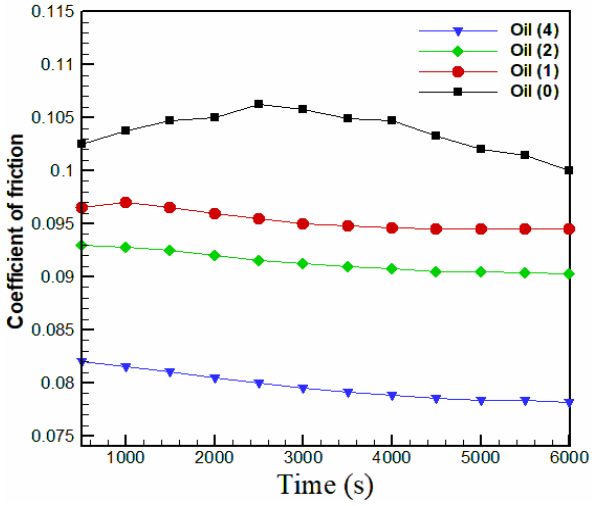

**Fig. 9.** Friction coefficient of the base oil and oils containing $WS_2$, $WS_2$-2, and $WS_2$-4 nanoflakes

Wu et al. synthesized nano-$WS_2$ + ionic liquid with a 0.13 friction coefficient [67]. Zhang et al. investigated $WS_2$ Nanosheets and found a 0.11 friction coefficient [68]. Jiang et al. studied Oleylamine-Modified Ultrathin $WS_2$ which friction coefficient was 0.10 [69]. The friction coefficient in this research is 0.082.

The wear scar diameter (WSD) can be calculated according to the details in reference [70]. It can be seen that the WSDs in the attendance of the additives is reduced (Table 2). The maximum reduction is 54% for Oil (4) compared to base Oil (0). Lane first introduced the Flash temperature parameter (FTP) [71]. FTP is the limited temperature at which oil causes lubricating films to flow properly. A higher FTP value indicates better lubrication performance. While the FTP value is low, the lubrication films will break and, therefore, the performance of the lubrication will be inadequate. The FPT is related to the load and amount of WSD applied as follows:

$$\mathrm{FTP}=\frac{Applied\ load}{(Wear\ scar\ diameter)^{1.4}}=\frac{W}{d^{1.4}} \quad (2)$$

Where W is the applied load in kilograms and d is the value of WSD in millimeters. The results of FTP calculation with 40 kg load applied are shown in Table 2. FTP of oil (4) increased by 82.7% compared to a base Oil (0). According to the above results, the anti-wear property increased and the coefficient of friction decreased significantly for the $WS_2$ -4 sample.

**Table 2**
WSD and FTP of the samples

| Sample | WSD (mm) | FTP (kg/mm$^{1.4}$) |
|---|---|---|
| Oil(0) | 0.321 | 215.81 |
| Oil(1) | 0.265 | 265.75 |
| Oil(2) | 0.230 | 313.06 |
| Oil(4) | 0.195 | 394.46 |

## 4. Conclusions

In this work, the $WS_2$ nanoflakes were successfully synthesized by the hydrothermal method. Freezing and heating methods were used to increase the liquid phase peeling of $WS_2$. To our knowledge, this method has not been used for $WS_2$. $WS_2$ was easily peeled off by cooling $WS_2$ powder in ethanol solvent under liquid nitrogen and heating by microwave irradiation. $WS_2$ peeling was confirmed using morphological examinations. Results showed that the optical bandgap of the bulk $WS_2$ (1.2 eV) increased up to 4.7 eV by increasing the round of the liquid nitrogen-microwave. The increase in the bandgap of a semiconductor has drastic changes in electrical and optical properties. The bandgap is a critical parameter from the application point of view. Moreover, such a large bandgap can be used to fabricate blue LEDs, laser diodes, high-temperature electronics, sensors, microprocessors, and ultraviolet LEDs with wavelengths down to 200–250 nm. The tribological properties of the $WS_2$ nanoflakes as additives in oil were investigated at room temperature. The results showed that the friction coefficient reduced, and the wear scars decreased by approximately 54% for Oil (4) compared to the base Oil (0). Thus, fabricated specimens have the potential to play a role in lowering friction and anti-wear when used as an additive in base oils. In addition, this process is cost-effective, environmentally pleasant, and easy to produce on a large scale.

## References

[1] M. Ali, H. Xianjun, Improving the tribological behavior of internal combustion engines via the addition of nanoparticles to engine oils, Nanotechnol, A 4 (2015) 347.

[2] J. Kogovšek, M. Kalin, Various $MoS_2$-, $WS_2$- and C-Based Micro- and Nanoparticles in Boundary Lubrication, Tribol. Lett, A 53 (2014) 585.

[3] E. Ettefaghi, H. Ahmadi, A. Rashidi, A. Nouralishahi, S. Mohtasebi, Preparation and thermal properties of oil-based nanofluid from multi-walled carbon nanotubes and engine oil as nano-lubricant, INT COMMUN HEAT MASS, A 46 (2013) 142.

[4] H. Fu, G. Yan, M. Li, H. Wang, Y. Chen, C. Yan, C. Lin, N. Jiang, J. Yu, Graphene as a nanofiller for enhancing the tribological properties and thermal conductivity of base grease, RSC Adv, A 72 (2019) 42481.

[5] C. Altavilla, M. Sarno, P. Ciambelli, A. Senatore, V. Petrone, New 'chimie douce' approach to the synthesis of hybrid nanosheets of $MoS_2$on CNT and their anti-friction and anti-wear properties, Nanotechnology, A 24 (2013) 125601.

[6] N. Win Khun, H. Zhang, L. Hoon Lim, J. Yang, Mechanical and Tribological Properties of Graphene Modified Epoxy Composites, (KMUTNB) Int. J. App. Sci, A 8 (2015) 101.

[7] E. Hu, Y. Xu, K. Hu, X. Hu, Tribological properties of 3 types of $MoS_2$ additives in different base greases, LUBR SCI, A 29 (2017) 541.

[8] M. Charoo, M. Wani, M. Hanief, M. Rather, Tribological Properties of $MoS_2$ Particles as Lubricant Additive on EN31 Alloy Steel and AISI 52100 Steel Ball, Proceedings, A 4 (2017) 9967.

[9] Y. Wu, H. Li, L. Ji, L. Liu, Y. Ye, J. Chen, H. Zhou, Structure, Mechanical, and Tribological Properties of $MoS_2$/a-C:H Composite Films, Tribol. Lett, A 52 (2013) 371.

[10] M. Ratoi, V. Niste, J. Walker, J. Zekonyte, Mechanism of Action of $WS_2$ Lubricant Nanoadditives in High-Pressure Contacts, Tribol. Lett, A 52 (2013) 81.

[11] I. Jenei, F. Svahn, S. Csillag, Correlation Studies of WS 2 Fullerene-Like Nanoparticles Enhanced Tribofilms: A Scanning Electron Microscopy Analysis, Tribol. Lett, A 51 (2013) 461.

[12] P. Aldana, B. Vacher, T. Le Mogne, M. Belin, B. Thiebaut, F. Dassenoy, Action Mechanism of WS2 Nanoparticles with ZDDP Additive in Boundary Lubrication Regime, Tribol. Lett, A 56 (2014) 249.

[13] V. Niste, H. Tanaka, M. Ratoi, J. Sugimura, WS2 nano additive lubricant for applications affected by hydrogen embrittlement, RSC Adv, A 5 (2015) 40678.

[14] S. Ingole, A. Charanpahari, A. Kakade, S. Umare, D. Bhatt, J. Menghani, Tribological behavior of nano TiO2 as an additive in base oil, Wear, A 301 (2013) 776.
[15] A. Hernandez Battez, J. Fernandez Rico, A. Navas Arias, J. Viesca Rodriguez, R. Chou Rodriguez, J. Diaz Fernandez, The tribological behavior of ZnO nanoparticles as an additive to PAO6, Wear, A 261 (2006) 256.
[16] J. Guo, G. Barber, D. Schall, Q. Zou, S. Jacob, Tribological properties of ZnO and $WS_2$ nanofluids using different surfactants, Wear, A15 (2017) 382.
[17] L. Gara, Q. Zou, Friction and Wear Characteristics of Oil-Based ZnO Nanofluids, Tribology T, A 56 (2013) 236.
[18] L. Taran, R. Rasuli, Cost-effective liquid-phase exfoliation of molybdenum disulfide by prefreezing and thermal-shock, ADV POWDER TECHNOL, A 28 (2017) 2996.
[19] B. Li, X. Wang, W. Liu, Q. Xue, Tribochemistry and antiwear mechanism of organic–inorganic nanoparticles as lubricant additives, Tribol. Lett, A 22 (2006) 79.
[20] Lince, Jeffrey R. "Effective application of solid lubricants in spacecraft mechanisms." Lubricants 8, 7 (2020) 74.
[21] Freschi, Marco, Matteo Di Virgilio, Gabriele Zanardi, Marco Mariani, Nora Lecis, and Giovanni Dotelli. "Employment of Micro-and Nano-$WS_2$ Structures to Enhance the Tribological Properties of Copper Matrix Composites." Lubricants 9, 5 (2021) 53.
[22] Fayaz, Syed Danish, and M. F. Wani. "Insights into the tribological behavior of IF-$WS_2$ nanoparticle reinforced mild extreme pressure lubrication for coated chromium/bulk grey cast iron interface." Proceedings of the Institution of Mechanical Engineers, Part J: Journal of Engineering Tribology (2021) 1350650120964026.
[23] N. Wu, N. Hu, J. Wu, G. Zhou, Tribology Properties of Synthesized Multiscale Lamellar $WS_2$ and Their Synergistic Effect with Anti-Wear Agent ZDDP, Appl. Sci, A 10 (2019) 115.
[24] X. Zhu, J. Yang, X. She, Y. Song, J. Qian, Y. Wang, H. Xu, H. Li, Q. Yan, Rapid synthesis of ultrathin 2D materials through liquid-nitrogen and microwave treatments, J. mater. chem, A 7 (2019) 5209.
[25] Q. Wang, K. Kalantar-Zadeh, A. Kis, J. Coleman, M. Strano, Electronics and optoelectronics of two-dimensional transition metal dichalcogenides, Nat. Nanotechnol, A 7 (2012) 699.
[26] S. Cao, T. Liu, S. Hussain, W. Zeng, X. Peng, F. Pan, Hydrothermal synthesis of variety low dimensional $WS_2$ nanostructures, Mater. Lett., A 129 (2014) 205.
[27] M. Piao, J. Chu, X. Wang, Y. Chi, H. Zhang, C. Li, H. Shi, M.K. Joo, Hydrothermal synthesis of stable metallic 1T phase $WS_2$ nanosheets for thermoelectric application, Nanotechnology, A 29 (2017) 025705.
[28] G. Cunningham, M. Lotya, C. Cucinotta, S. Sanvito, S. Bergin, R. Menzel, M. Shaffer, J. Coleman, Solvent Exfoliation of Transition Metal Dichalcogenides: Dispersibility of Exfoliated Nanosheets Varies Only Weakly between Compounds, ACS Nano, A 6 (2012) 3468.
[29] A. Winchester, S. Ghosh, S. Feng, A.L. Elias, T. Mallouk, M. Terrones, S. Talapatra, Electrochemical Characterization of Liquid Phase Exfoliated Two-Dimensional Layers of Molybdenum Disulfide, ACS APPL MATER INTER, A 6 (2014) 2125.
[30] K. Zhou, N. Mao, H. Wang, Y. Peng, H. Zhang, A Mixed-Solvent Strategy for Efficient Exfoliation of Inorganic Graphene Analogues, Chem. Int. Ed, A 123 (2011) 11031.
[31] U. Halim, C.R. Zheng, Y. Chen, Z. Lin, S. Jiang, R. Cheng, Y. Huang, X. Duan, A rational design of cosolvent exfoliation of layered materials by directly probing liquid–solid interaction, *Nat. Commun*, A 4 (2013) 1.
[32] X. Liu, J. Liu, D. Zhan, J. Yan, J. Wang, D. Chao, L. Lai, M. Chen, J. Yin, Z. Shen, Repeated microwave-assisted exfoliation of expandable graphite for the preparation of large scale and high-quality multi-layer graphene, RSC advances, A 3 (2013) 11601.
[33] Z. Liu, Y. Wang, Z. Wang, Y. Yao, J. Dai, S. Das, L. Hu, olvo-thermal microwave-powered two-dimensional material exfoliation, ChemComm, A 33 (2016) 5757.
[34] A. Albu-Yaron, M. Levy, R. Tenne, R. Popovitz-Biro, M. Weidenbach, M. Bar-Sadan, L. Houben, A. Enyashin, G. Seifert, D. Feuermann, E. Katz, J. Gordon, $MoS_2$ Hybrid Nanostructures: From Octahedral to Quasi-Spherical Shells within Individual Nanoparticles, Angew. Chem. Int. Ed, A 8 (2011) 1810.
[35] Y. Lin, D. Dumcenco, Y. Huang, K. Suenaga, Atomic mechanism of the semiconducting-to-metallic phase transition in single-layered MoS2, Nat. Nanotechnol, A 9 (2014) 391.
[36] K. Peng, H. Wang, X. Li, J. Wang, Z. Cai, L. Su, X. Fan, Emerging $WS_2$/montmorillonite composite nanosheets as an efficient hydrophilic photocatalyst for aqueous phase reactions, Sci. Rep, A 9 (2019) 1.
[37] S. Hazarika, D. Mohanta, norganic fullerene-type $WS_2$ nanoparticles: processing, characterization and its photocatalytic performance on malachite green, APPL PHYS A, A 123 (2017) 381.
[38] X. Zhang, J. Wang, H. Xu, H. Tan, X. Ye, Preparation and Tribological Properties of $WS_2$ Hexagonal Nanoplates and Nanoflowers, *Nanomaterials*, A 9 (2019) 840.
[39] Q. Pang, Y. Gao, Y. Zhao, Y. Ju, H. Qiu, Y. Wei, B. Liu, B. Zou, F. Du, G. Chen, improved Lithium-Ion and Sodium-Ion Storage Properties from Few-Layered $WS_2$ Nanosheets Embedded in a Mesoporous CMK-3 Matrix, Chem. Eur. J, A 23 (2017) 7074.
[40] X. Zhao, X. Ma, J. Sun, D. Li, X. Yang, Enhanced Catalytic Activities of Surfactant-Assisted Exfoliated $WS_2$ Nanodots for Hydrogen Evolution, ACS Nano, A 10 (2016) 2159.
[41] B. Mahler, V. Hoepfner, K. Liao, G. Ozin, Colloidal Synthesis of 1T-$WS_2$ and 2H-$WS_2$ Nanosheets: Applications for Photocatalytic Hydrogen Evolution, J. Am. Chem. Soc, A 136 (2014) 14121.
[42] S. Sharma, S. Bhagat, J. Singh, R. Singh, S. Sharma, Excitation-dependent photoluminescence from $WS_2$ nanostructures synthesized via top-down approach, J. Mater. Sci, A 52 (2017) 11326.

[43] S. Vattikuti, C. Byon, Effect of CTAB Surfactant on Textural, Structural, and Photocatalytic Properties of Mesoporous $WS_2$, Sci. Adv. Mater, A 7 (2015) 2639.
[44] J. Wu, G. Yue, Y. Xiao, M. Huang, J. Lin, L. Fan, Z. Lan, J. Lin, Glucose Aided Preparation of Tungsten Sulfide/Multi-Wall Carbon Nanotube Hybrid and Use as Counter Electrode in Dye-Sensitized Solar Cells, ACS APPL MATER INTER, A 4 (2012) 6530.
[45] R. A. Ismail, G. M. Sulaiman, S. A. Abdulrahman, T. R. Marzoog, Solvothermal synthesis of Au@$Fe_3O_4$ nanoparticles for antibacterial applications, Mater. Sci. Eng., C, 53 (2015) 286–297.
[46] Li N. Chen, J. Shi, Y.-P. Anal. Magnetic polyethyleneimine functionalized reduced graphene oxide as a novel magnetic solid-phase extraction adsorbent for the determination of polar acidic herbicides in rice, Chim. Acta, 949 (2017) 23–34.
[47] Y. Yan, C. Zhang, W. Gu, C. Ding, X. Li, Y. Xian, Facile Synthesis of Water-Soluble $WS_2$ Quantum Dots for Turn-On Fluorescent Measurement of Lipoic Acid, J. Phys. Chem C, A 120 (2016) 12170.
[48] A. Bayat, E. Saievar-Iranizad, Synthesis of blue photoluminescent $WS_2$ quantum dots via ultrasonic cavitation, J. Lumin, A 185 (2017) 236.
[49] G. Frey, S. Elani, M. Homyonfer, Y. Feldman, R. Tenne, Optical-absorption spectra of inorganic fullerenelike $MS_2$ (M=Mo,W), Phys. Rev, A 57 (1998) 6666.
[50] K. He, N. Kumar, L. Zhao, Z. Wang, K. Mak, H. Zhao, J. Shan, Tightly Bound Excitons in Monolayer$WSe_2$, PHYS REV LETT, A 113 (2014) 026803.
[51] S. Xu, D. Li, P. Wu, One-Pot, Facile, and Versatile Synthesis of Monolayer $MoS_2$/$WS_2$ Quantum Dots as Bioimaging Probes and Efficient Electrocatalysts for Hydrogen Evolution Reaction, Adv. Funct. Mater, A 25 (2015) 1127.
[52] H. Mishra, S. Umrao, J. Singh, R. Srivastava, R. Ali, A. Misra, A. Srivastava, pH Dependent Optical Switching and Fluorescence Modulation of Molybdenum Sulfide Quantum Dots, Advanced Optical Materials 5, 9 (2017) 1601021.
[53] F. Laatar, M. Hassen, C. Amri, F. Laatar, A. Smida, H. Ezzaouia, Fabrication of CdSe nanocrystals using porous anodic alumina and their optical properties, J. Lumin, A 178 (2016) 13.
[54] N. Ben Brahim, M. Poggi, N. Haj Mohamed, R. Ben Chaâbane, M. Haouari, M. Negrerie, H. Ben Ouada, Synthesis, characterization and spectral temperature-dependence of thioglycerol-CdSe nanocrystals, J. Lumin, A 177 (2016) 402.
[55] Y. Sang, Z. Zhao, M. Zhao, P. Hao, Y. Leng, H. Liu, From UV to Near-Infrared, $WS_2$ Nanosheet: A Novel Photocatalyst for Full Solar Light Spectrum Photodegradation, Adv. Mater, A 27 (2015) 363.
[56] S. Notley, High yield production of photoluminescent tungsten disulphide nanoparticles, J. Colloid Interface Sci, A 15 (2013) 160.
[57] H. Jiang, Electronic Band Structures of Molybdenum and Tungsten Dichalcogenides by the GW Approach, J. Phys. Chem, A 116 (2012) 7664.
[58] D. Feng, Z. Xu, T. Jia, X. Li, S. Gong, Quantum size effects on exciton states in indirect-gap quantum dots, Phys. Rev B, A 68 (2003) 035334.
[59] X. Duan, Q. Liu, G. Wang, X. Su, $WS_2$ quantum dots as a sensitive fluorescence probe for the detection of glucose, MICROCHIM ACTA, A 207 (2019) 491.
[60] Lin, T. N., S. R. M. Santiago, S. P. Caigas, C. T. Yuan, T. Y. Lin, J. L. Shen, and Y. F. Chen. "Many-body effects in doped $WS_2$ monolayer quantum disks at room temperature." npj 2D Materials and Applications 3, 1 (2019) 1-6.
[61] Y. S. Liu, X. M. Hu, T. Wang, and D. M. Liu, "Reduced Binding Energy and Layer-Dependent Exciton Dynamics in Monolayer and Multilayer $WS_2$," ACS Nano 13(12) (2019) 14416–14425.
[62] A. Hichri, I. B. Amara, S. Ayari, and S. Jaziri, "Dielectric environment and/or random disorder effects on free,charged and localized excitonic states in monolayer $WS_2$," J. Phys.: Condens. Matter 29(43) (2017) 435305.
[63] Xu, Xuejun, Lihui Li, Mingming Yang, Qinglin Guo, Ying Wang, Xiaoli Li, Xiujuan Zhuang, and Baolai Liang. "Localized state effect and exciton dynamics for monolayer $WS_2$." Optics Express 29, 4 (2021) 5856-5866.
[64] H. Wang, C. Zhang, W. Chan, S. Tiwari, F. Rana, Ultrafast response of monolayer molybdenum disulfide photodetectors, A 6 (2015) 339.
[65] Ma, Churong, Jiahao Yan, Yingcong Huang, and Guowei Yang. Photoluminescence manipulation of $WS_2$ flakes by an individual Si nanoparticle, Materials Horizons 6, 1 (2019) 97-106.
[66] M. Mahdavi, S. Kimiagar, and F. Abrinaei, Effect of Laser Energy on the Tribology Properties of $MoS_2$ Flakes, Tribology in Industry 42(2) (2020).
[67] Wu, Na, Ningning Hu, Gongbo Zhou, and Jinhe Wu. "Tribological properties of lubricating oil with micro/nano-scale $WS_2$ particles." Journal of Experimental Nanoscience 13, 1 (2018) 27-38.
[68] Zhang, Xianghua, Hongxiang Xu, Jiangtao Wang, Xia Ye, Weining Lei, Maoquan Xue, Hua Tang, and Changsheng Li. "Synthesis of ultrathin $WS_2$ nanosheets and their tribological properties as lubricant additives." Nanoscale research letters 11, 1 (2016) 1-9.
[69] Jiang, Zhengquan, Yujuan Zhang, Guangbin Yang, Kunpeng Yang, Shengmao Zhang, Laigui Yu, and Pingyu Zhang. "Tribological properties of oleylamine-modified ultrathin $WS_2$ nanosheets as the additive in polyalpha olefin over a wide temperature range." Tribology Letters 61, 24 (2016) 3.
[70] A. Bos, Wear in the four-ball apparatus: relationship between the displacement of the upper ball and the diameter of the wear scars on the lower balls, Wear, A 41 (1977) 191.
[71] T.B. Lane, the flash temperature parameter: A criterion for assessing EP performance in the four-ball machine, J JPN PETROL INST, A 4 (1961) 254.